Chem Catalysis

Article

Zeolite composite prepared by quasi-*in situ* interzeolite conversion approach

Graphical abstract

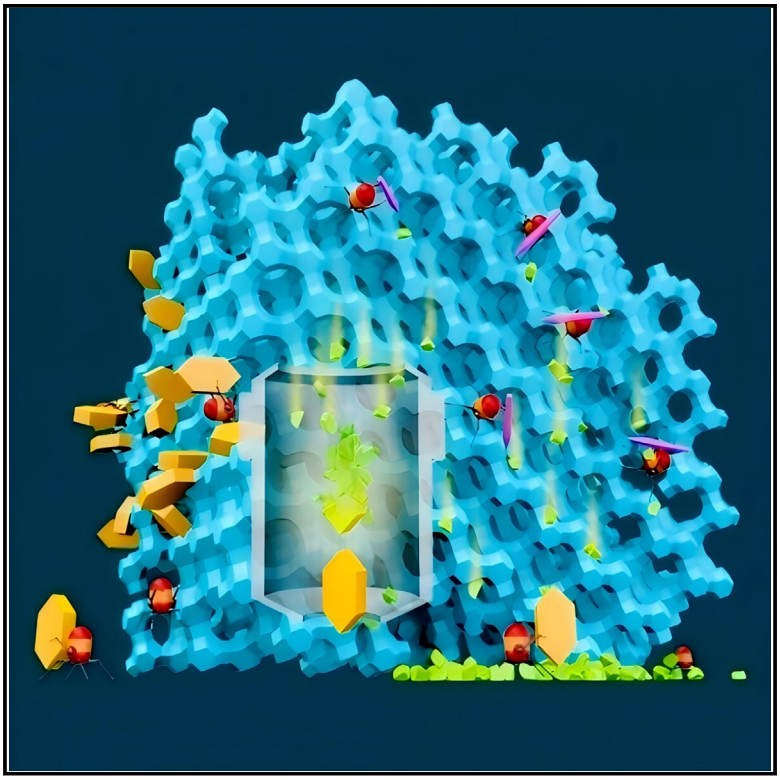

Highlights

- Quasi-*in situ* interzeolite conversion produces mesoporous Y/ZSM-5 composites
- Confined mass transfer enables hierarchical USY and nanosized ZSM-5 integration
- Tunable zeolite ratio tailors properties for catalytic applications

Authors

Ruizhe Zhang, Bo Wang, Jiani Xu, ..., Zhengxing Qin, Xionghou Gao, Svetlana Mintova

Correspondence

zhengxing.qin@upc.edu.cn (Z.Q.), gaoxionghou@petrochina.com.cn (X.G.), svetlana.mintova@ensicaen.fr (S.M.)

In brief

Composite zeolites, valued for their synergistic effects, unique pore structures, and abundant active sites, show promise in enhancing practical applications. However, their industrial use faces limitations due to complex preparation and harsh synthesis conditions. Here, we propose a quasi-*in situ* interzeolite conversion method to synthesize hierarchical Y/nano-ZSM-5 composites. This approach enables precise control over the two-phase zeolite ratio, offering a versatile and efficient route for preparing hierarchical composites, particularly for catalytic applications.

Zhang et al., 2025, Chem Catalysis *5*, 101298
May 15, 2025
https://doi.org/10.1016/j.checat.2025.101298

CellPress

Please cite this article in press as: Zhang et al., Zeolite composite prepared by quasi-*in situ* interzeolite conversion approach, Chem Catalysis (2025), https://doi.org/10.1016/j.checat.2025.101298

Chem Catalysis

CellPress

Article

Zeolite composite prepared by quasi-*in situ* interzeolite conversion approach

Ruizhe Zhang,[1,2,8] Bo Wang,[1,8] Jiani Xu,[1,3] Honghai Liu,[4] Hongjuan Zhao,[4] Jiujiang Wang,[4] Shutao Xu,[3] Shunsuke Asahina,[5] Francesco Dalena,[2] Camille Longue,[2,6] Benoît Louis,[6] Ludovic Pinard,[2] Simona Moldovan,[7] Zhengxing Qin,[1,*] Xionghou Gao,[4,*] and Svetlana Mintova[1,2,9,*]

[1]State Key Laboratory of Heavy Oil Processing, College of Chemistry and Chemical Engineering, China University of Petroleum (East China), Qingdao 266580, China

[2]Laboratoire de Catalyse et Spectrochimie, LCS, UMR 6506, ENSICAEN, Caen, France

[3]National Engineering Research Center of Lower-Carbon Catalysis Technology, Dalian Institute of Chemical Physics, Chinese Academy of Sciences, Dalian, Liaoning 116023, China

[4]Petrochemical Research Institute, PetroChina Company Limited, Beijing 100195, China

[5]Advanced Material Analysis Co-creation Research Center, Institute of Multidisciplinary Research for Advanced Materials, Tohoku University, Sendai, Japan

[6]Institut de Chimie et Procédés pour l'Energie, l'Environnement et la Santé, ICPEES, UMR 7515, Université de Strasbourg-ECPM, Strasbourg, France

[7]Groupe de Physique des Matériaux, CNRS, University Rouen Normandie, INSA Rouen Normandie, UMR 6634, 76000 Rouen, France

[8]These authors contributed equally

[9]Lead contact

*Correspondence: zhengxing.qin@upc.edu.cn (Z.Q.), gaoxionghou@petrochina.com.cn (X.G.), svetlana.mintova@ensicaen.fr (S.M.)

https://doi.org/10.1016/j.checat.2025.101298

THE BIGGER PICTURE With the growing emphasis on sustainable production and an evolving energy landscape, zeolite research is presented with both opportunities and challenges. A major limitation of traditional zeolites is their narrow micropores, which restrict intra-particle diffusion efficiency. To address this, current strategies focus on synthesizing nano- or hierarchical zeolites or developing zeolites with larger micropores. Combining different types of zeolites offers a synergistic "1 + 1 > 2" effect, where pores of varying sizes and topologies enhance molecular diffusion, resulting in unique catalytic activity and selectivity in separation. Here, we introduce a quasi-*in situ* interzeolite conversion method for synthesizing Y/ZSM-5 composites with upgraded mesoporosity and improved pore connectivity. This method enables precise control of the relative concentrations of the two zeolites in the composite, allowing tailored properties for specific applications. We propose that this quasi-interzeolite conversion strategy serves as a versatile route for creating hierarchical composites, unlocking their potential in catalysis and adsorption processes critical to sustainable technologies.

SUMMARY

The design of zeolites with optimized textural properties is a continuous goal. Here, we report a composite comprising mesoporous ultra-stable zeolite Y (USY) and nanosized Zeolite Socony Mobil-5 (ZSM-5) with enhanced acid site accessibility and pore connectivity through quasi-*in situ* interzeolite conversion in a solvent-free medium. The preparation of the composite begins with a spatial and elemental-biased dissolution of USY with impregnated tetrapropylammonium hydroxide (TPAOH). This results in a hierarchical zeolite with increased mesopore volume and improved pore connectivity. Simultaneously, the solute provides all the necessary nutrients for the growth of ZSM-5 zeolite. Due to the constrained mass transfer during the quasi-solid-state dissolution, the resulting ZSM-5 crystals are as small as 10 nm and intimately connected with the USY zeolite. The advantageous synergy between zeolites Y and ZSM-5 in the composite was demonstrated through the methanol-to-olefin reaction and the cracking of n-hexane.

Please cite this article in press as: Zhang et al., Zeolite composite prepared by quasi-*in situ* interzeolite conversion approach, Chem Catalysis (2025), https://doi.org/10.1016/j.checat.2025.101298

INTRODUCTION

Zeolites have been used as solid acid catalysts in several large-scale industrial processes for more than 50 years, thanks to their outstanding (hydro)thermal stability, unique shape selectivity, and strong acidity.[1–4] With the increasing focus on sustainable production in industry and the evolving energy landscape, zeolite research faces both new opportunities and challenges. Breakthroughs in this field depend on factors such as performance, synthesis costs, scalability, environmental impact, and recyclability.[5–10] One of the obstacles that zeolites must overcome, especially during the handling of bulky reactant molecules, is the limited intra-particle diffusion efficiency imposed by their narrow micropores. To address this long-standing issue, there is a sustained effort to explore new zeolite structures with intrinsically larger micropores, able to process bulkier molecules.[11] However, significant efforts have also been made to improve mass transport in zeolites[12,13] through the synthesis of zeolites with nanosized dimensions, or the preparation of hierarchical zeolites featuring an auxiliary macro- and/or mesoporous network. Classical examples include but are not limited to the direct synthesis of embryonic or fully crystalline zeolites with at least one dimension in ultra-small size.[14,15]

Among the cases summarized above, we are dealing with only one type of zeolite framework at a time. Whether using direct synthesis with or without structural templating or post-synthetic modifications such as dealumination, desilication, or demetallation, we typically focus on engineering the mass transfer properties of a single zeolite framework. In practice, the combination of two or more types of zeolites often produce a "1 + 1 > 2" synergy effect,[16–21] as the presence of pores of varied sizes and topologies would favor the preferential diffusion of molecules through the different pore systems, allowing unique activity and selectivity in some specific catalysis and separation applications.[22–25] For example, the combined use of Cu-Zn-Al oxide/H-ZSM-5 (Zeolite Socony Mobil-5) and H-MOR catalysts exhibits high methyl acetate and acetic acid selectivity (~95%) in the conversion of syngas into C_2^+ oxygenates.[18] Among others, a typical example is the combined use of Y and ZSM-5 zeolites in fluid catalytic cracking (FCC).[19] In FCC catalysts, Y zeolite functions as the core component of catalytic cracking,[26,27] and ZSM-5 zeolite was used as an additive to enhance propylene selectivity.[28,29]

In this context, researchers were driven to investigate numerous synthesis methods for Y/ZSM-5 composites, demonstrating their performance. For instance, Shen et al.[30] utilized a two-step crystallization process, employing tetraethylammonium bromide and tetrabutylammonium bromide as structure-directing agents, to synthesize ZSM-5/Y composite zeolite based on the initial synthesis of Y zeolite. The study revealed that compared with a mechanically mixed sample with the same phase ratio, the zeolite composite exhibited higher diesel and light olefin yields in catalytic cracking reactions, alongside lower gasoline yields and feedstock conversion rates. Similarly, Li and coworkers explored various methods to prepare Y/ZSM-5 composites. Through the attachment growth of Y-type zeolite seeds, they prepared a composite where Y zeolite was uniformly attached to the surface of ZSM-5 zeolite.[31] This introduced a multi-level pore structure into the composite, enhancing mass transfer efficiency, conversion rate, and catalyst lifespan in the triisopropylbenzene reaction. Furthermore, by controlling the overgrowth of another zeolite shell on the surface of zeolite Y, a novel core-shell catalyst was developed, improving the heavy oil conversion rate and olefin yield in the vacuum gas oil catalytic cracking process.[32]

Despite these advancements, the industrial use of Y/ZSM-5 composite zeolite still faces the problems of complicated preparation processes, complex raw materials sources, and harsh synthesis conditions. The industrial FCC catalysts are prepared by synthesizing two zeolites separately, modifying them through post-treatment, and subsequently mixing them to enhance catalytic performance.[17,33]

Here, we report the preparation of zeolite composite composed of hierarchical zeolite Y and nanosized ZSM-5 zeolite by the quasi-*in situ* interzeolite conversion approach. This is achieved through the partial interzeolite conversion from zeolite Y to ZSM-5, resulting in the composite (Figure 1; Video S1). Unlike other protocols that transfer a zeolite framework to an amorphous derivative[34] or a different crystalline framework with a distinct topology,[35] the strategy reported in the present work is unique and is referred to as quasi-*in situ* interzeolite conversion. It involves a controlled dissolution of the parent zeolite Y, which not only facilitates the formation of highly mesoporous zeolite but also supplies all the necessary nutrients for the crystallization of ZSM-5 zeolite. Moreover, as the strategy is a quasi-*in situ* interzeolite conversion, the mass transfer of the dissolved species is substantially restricted. This results in the synthesis of ZSM-5 zeolite with ultra-small nanocrystals.

RESULTS AND DISCUSSION

XRD and NMR

The X-ray diffraction (XRD) pattern of the parent ultra-stable Y zeolite (USY) confirms the high crystallinity of the sample (Figure 2). The attempt to transform it into a composite was not successful. The sample remained stable, and Bragg peak intensity changed insignificantly after the high-temperature hydrothermal treatment in the presence of tetrapropylammonium hydroxide (TPAOH) (Figure S1). It is probable that the Si/Al ratio of the commercial USY zeolite sample is too low to be dissolved considerably in the applied alkaline treatment condition.[36] The presence of TPA^+ provides an additional protection to the zeolite treated in an alkaline medium, as already reported for other materials.[37]

To enhance the reactivity of the USY zeolite in an alkaline media, it was subjected to acid leaching (see methods). The resulting USY-A (A for acid leaching) sample exhibits high crystallinity and purity, as shown by XRD. A slight right shift of the Bragg peak compared to the parent USY zeolite is observed (Figures 2 and S2). In line with the rightward shift of the XRD peaks, the bulk Si/Al ratio of the USY and USY-A zeolites changed from 6.1 to 22.7 (Table 1). Both extra-framework Al (EFAL) and framework-connected Al were extracted during the acid treatment. This is stated based on the results obtained from the ^{27}Al magic angle spinning (MAS) NMR spectra (Figure 3A). In the parent USY zeolite, there are framework tetrahedral coordinated Al species (peaked at ~60 ppm), distorted tetrahedral Al species (30- to 50-ppm region), and octahedral coordinated Al species (peaked at 0 ppm),[38,39] and

Please cite this article in press as: Zhang et al., Zeolite composite prepared by quasi-*in situ* interzeolite conversion approach, Chem Catalysis (2025), https://doi.org/10.1016/j.checat.2025.101298

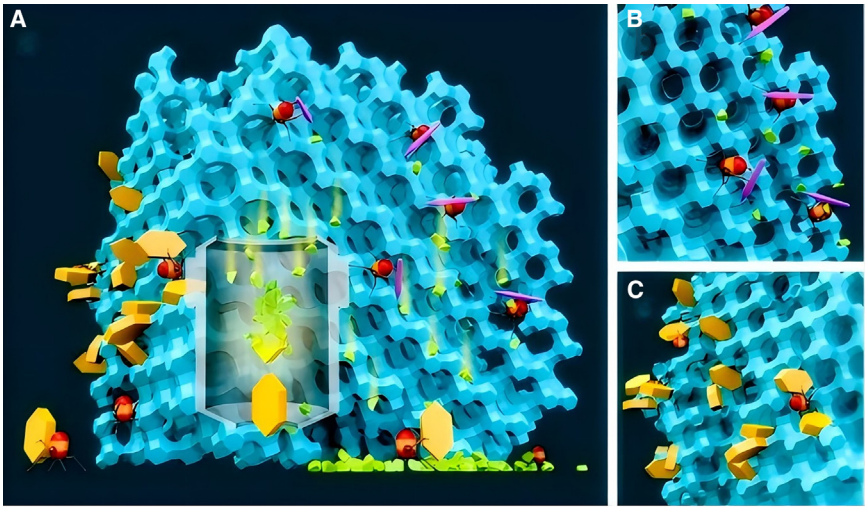

Figure 1. Graphical illustration of the methodology

(A) Overview of the quasi-*in situ* interzeolite conversion method used for preparing the Y/ZSM-5 composite.

(B and C) Partial dissolution of the USY zeolite framework (B) and formation of nanosized ZSM-5 zeolite (C), both induced by the TPAOH and hydrothermal environment. See also Video S1.

the estimated percentages of these species are ~39%, ~29%, and ~32%, respectively. The acid leaching removes a large portion of the EFAL species, including distorted tetrahedral and octahedral Al sites. In the USY-A sample, the amount of framework tetrahedral, distorted tetrahedral, and octahedral Al species is ~50%, ~29%, and ~21%, respectively.

The XRD pattern of the composite contains the Bragg peaks corresponding to zeolite Y, with a substantial decrease in intensity, and additional peaks characteristic of ZSM-5 zeolite occur accordingly. Based on the XRD results, the composite consists of 40% Y and 60% ZSM-5 phases. The ^{27}Al and ^{29}Si MAS NMR results (Figure 3) provide additional evidence for the presence of ZSM-5 in the composite. Specifically, the ^{27}Al MAS NMR spectrum shows a bifurcated resonance between 40 and 70 ppm, which is a clear indication for the presence of two types of framework Al species with distinct chemical shifts. The deconvolution of this peak revealed two components: a low-field signal centered at 60.4 ppm and a high-field signal at 54.1 ppm (Figure 3A). The calculated proportions for these two peaks are 32% and 68%, respectively. Assuming that the ^{27}Al MAS NMR resonance at 40–70 ppm is associated with the tetrahedrally coordinated Al species in Y and ZSM-5 zeolites, the calculated relative proportion between Y and ZSM-5 is quite different from that estimated ones based on the XRD data. This discrepancy is tentatively attributed to the incomplete conversion from zeolite Y to ZSM-5—namely, not all the tetrahedral coordinated Al species are situated in the framework tetrahedral position. As far as the ^{29}Si MAS NMR is concerned, the quasi-interzeolite conversion also results in a change in the shape of the spectra (Figure 3B). Two new peaks appear at −116.0 and −112.7 ppm, corresponding to the formation of ZSM-5 after interzeolite conversion.[34,40] The Si/Al ratio of the composite based on the ^{29}Si MAS NMR is 26.6.

N_2 and Ar physisorption

The change in the porosity of the samples was studied using N_2 physisorption. The isotherm of the USY-A zeolite, shown in Figure 4A is a typical type IV(a) isotherm, indicating the presence of both micropores and mesopores. The amount of N_2 sorption at a relative pressure (P/P_0) below 0.1 is relatively high for the pure Y zeolite.[12] The high micropore volume (Table 1) suggests that the acid-treated sample USY-A contains pores wider than its intrinsic micropores or possibly narrow mesopore.[41] The occurrence of this secondary porosity is attributed to the acid leaching that partially removes the framework and EFAL from the parent USY zeolite (Figure 3A). This is clearly illustrated in Figure 4A. The pore size distribution curves of the three samples are depicted in Figure 4B.

After interzeolite conversion, the micropore volume of the composite as determined by *t* plot, is 0.20 $cm^3\ g^{-1}$, which is a 45% decrease compared to the parent USY-A zeolite. This is partially because the micropore volume of a fully crystalline ZSM-5 zeolite is intrinsically smaller than that of the Y type zeolite.[42] Another hypothesis could be the formation of residual amorphous phase due to the incomplete interzeolite conversion—namely, not all aluminosilicate species dissolved from the parent USY zeolite are consumed and convert into ZSM-5 zeolite during the inter-conversion treatment. However, the mesopore volume of the Y/ZSM-5 composite increased by 100% in comparison to its reference sample (Table 1). The adsorption and desorption branches of the isotherms of the Y/ZSM-5 zeolites almost overlap with each other, with a continuously increasing sorption of N_2 in the whole P/P_0 range (Figure 4A). As a result, the pore size distribution of this sample is wide, and the sample is almost free of confined mesopores with narrow pore opening.[35,41]

The microporosity of samples was further analyzed by Ar physisorption. As the USY zeolite shows an initial sorption of Ar molecules at a relative pressure (P/P_0) higher than 1×10^{-4}, the initial point of physisorption of Ar molecules shift left to a P/P_0 lower than 1×10^{-4} in the case of USY-A, and further to a P/P_0 lower than 1×10^{-5} in the case of the Y/ZSM-5 composite, due to the sorption of Ar molecules in increasingly narrower micropores (Figure S3A). This is due to the difference in the intrinsic pore structure that ZSM-5 has a smaller micropore size than Y zeolite.[43]

SEM and TEM characterization

The morphology and structure of USY, USY-A zeolites, and Y/ZSM-composite were determined by scanning electron microscopy (SEM) and transmission electron microscopy (TEM) (Figures 5 and 6). Although the acid leaching results in an obvious increase in the micropore and mesopore volumes (Table 1),

Please cite this article in press as: Zhang et al., Zeolite composite prepared by quasi-*in situ* interzeolite conversion approach, Chem Catalysis (2025), https://doi.org/10.1016/j.checat.2025.101298

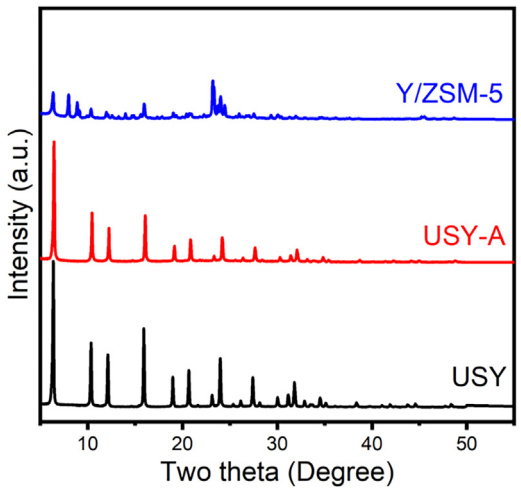

Figure 2. XRD patterns of parent USY, acid-treated zeolite USY-A, and the Y/ZSM-5 composite

both the USY and USY-A samples retain similar octahedral morphology characteristic of the faujasite (FAU)-type zeolite crystals (Figures 5A–5D). The crystal size, morphology, and density of the two samples USY and USY-A remain similar before and after the acid treatment, as characterized by TEM (Figures 6A–6D). These results are in good agreement with the N_2 physisorption data, as shown above. Apparently, the applied acid treatment mainly removes Al atoms from the zeolite framework, and EFAL species occluded inside the micropore and mesopores (Figure 3A). This could result in the opening of sodalite (SOD) cages[12] and the evacuation of existing mesopores, with increasing micropore volume (Table 1) instead of enlarging the mesopore sizes (Figure 4B).

The morphology of the zeolite sample changed substantially after the TPAOH-mediated interzeolite conversion. While the pure USY zeolites have an octahedral morphology with well-defined corners, edges, and facets (Figures 5A and 5B), these crystals become a minority in the case of the Y/ZSM-5 composite. The composite contains nanosized particles or porous fragments of irregular shape (Figures 5E and 5F). Like the results obtained by SEM, a diversified particle morphology is observed by TEM (Figures 6E and 6F). While some of the particles remain the morphology of USY zeolite crystals (Figure S4), there are also many fragmented particles. Noticeably, all the particles have a highly porous nature. A closer check at high magnification shows that these samples retain the high crystallinity (Figure S5). The high resistance of these crystals to leaching is elaborated further in the following section. Besides the presence of highly porous USY zeolite with diversified particle size and morphology, co-existing ZSM-5 zeolite crystals with a different morphology are present. The ZSM-5 zeolite nanocrystals form an open texture composed of oriented yet imperfectly attached nanocrystals. The dendritic structure clearly shows the front line of particle attachment and subsequent alignment (Figures 6E, 6F, S6, and S7). Apparently, crystal growth is hindered by the confined diffusion of aluminosilicate species detached from the USY zeolite. This results in the formation of ZSM-5 nanocrystals with a high crystallinity and porosity. This growth model is also predetermined by the absence of common construction building units between FAU- and MFI-type zeolites, which prevent the formation of intergrowth between the hierarchical Y and nano-ZSM-5 zeolites.

Based on the above SEM and TEM results, it has been observed that certain crystals retain an octahedral morphology that corresponds to the FAU type of zeolite following the quasi-interzeolite conversion process. However, the crystals exhibit an inhomogeneous density under TEM, with a higher density at the crystal periphery than in the central part (Figure S4). To gain insight into the surface and structural details, both the parent USY and the Y/ZSM-5 composite were studied further using high-resolution SEM. The parent USY zeolite is considered to be the reference sample, as the acid leaching has only a minor impact on the mesoporosity of the USY zeolite (Figures 6A–6D). In the case of the Y/ZSM-5 composite, special attention was paid to the zeolite crystals keeping the same morphology as the parent FAU-type zeolite. As can be seen from the high-resolution SEM images shown in Figure 7, there is no significant change in surface morphology between the parent USY and the composite. Both samples show a porous texture with a similar mesopore size. To observe the internal structure, both samples were cut using an Ar ion beam cross-section polisher equipped with a cooling system prior to SEM characterization. The cross-sectional view of USY zeolite shows the porous structure, and the contrast is uniform throughout the crystals. In comparison, the cross-section of the composite shows a lower density and the contrast varied due to the different porosity and thickness of the composite (Figures 7F and S8). The crystal periphery is more resistant to the post-synthesis treatment, and the dissolution probably starts preferentially from the inner part of the USY crystals during the interzeolite conversion. The preferential dissolution behavior can be rationalized by the fact that the outmost layer of zeolite crystals is formed during the last

Table 1. Physicochemical properties of samples

Sample	Si/Al[a]	Y/ZSM-5[b]	S_{BET},[c] m^2/g	S_{micro},[d] m^2/g	S_{meso},[e] m^2/g	V_{micro},[d] cm^3/g	V_{meso}[e] cm^3/g
USY	6.1	100: 0	867	812	55	0.31	0.14
USY-A	22.7	100: 0	985	912	73	0.36	0.20
Y/ZSM-5	20.1	40: 60	605	461	144	0.20	0.40

[a]Si/Al ratio determined from X-ray fluorescence.
[b]The ratio of the two zeolite components determined based on XRD.
[c]BET surface area.
[d]*t* plot method.
[e]$S/V_{meso} = S/V_{total} - S/V_{micro}$ (V_{total}: total pore volume calculated at $P/P_0 = 0.99$).

Please cite this article in press as: Zhang et al., Zeolite composite prepared by quasi-*in situ* interzeolite conversion approach, Chem Catalysis (2025), https://doi.org/10.1016/j.checat.2025.101298

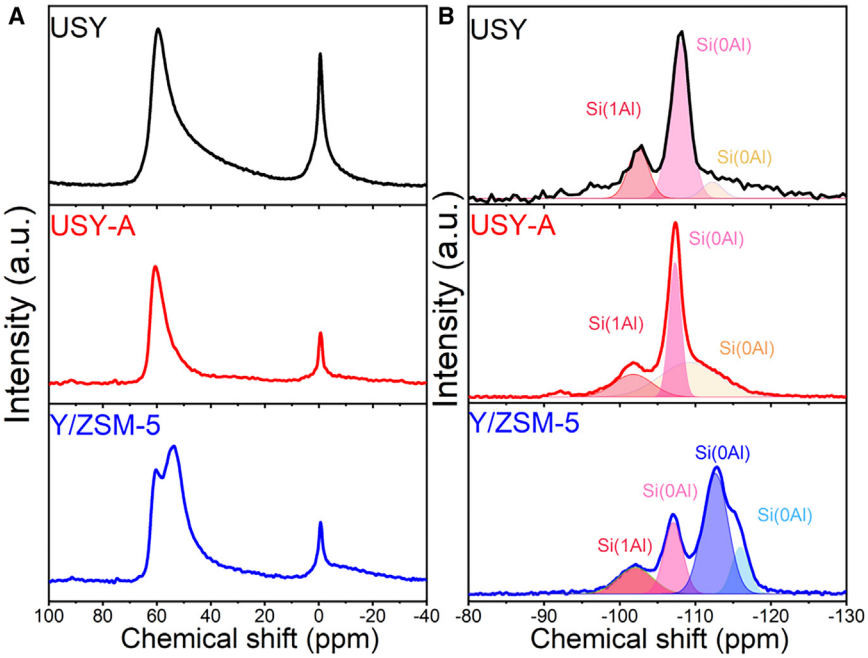

Figure 3. NMR study of the USY, USY-A, and Y/ZSM-5 composite

^{27}Al MAS NMR spectra (A) and ^{29}Si MAS NMR spectra (B, thick line) with corresponding deconvolution (B, thin lines) for the parent USY, acid-treated USY-A zeolites, and the Y/ZSM-5 composite.

stage of zeolite crystallization. In this case, fewer defects (or surface tension) are incorporated into the outermost layer of zeolite crystals.

The partial dissolution of zeolite crystals not only substantially improves the mesoporosity of the remaining zeolite Y crystals (Figures 6E and S4) but it also provides the nutrients for the growth of the ZSM-5 zeolite. Apparently, this is a single dissolution-recrystallization process that partially transform the zeolite Y into ZSM-5 zeolite, resulting in the Y/ZSM-5 zeolite composite in one step. An additional advantage of this synthesis approach is that almost no loss of Al and Si elements and nearly zero wastewater occurs, thanks to the application of the so-called solid-phase transformation. The crystalline yield of the Y/ZSM-5 composite ranges from 94% to 98%. The growth of ZSM-5 zeolite crystals is delayed due to the migration of nutrients from the treated USY-A sample. As a result, a dendritic-like crystal growth for the composite is observed that shapes the hierarchical structure made of USY zeolite consisting of ultrasmall nano-ZSM-5 zeolite crystals.

Electron tomography assays in scanning TEM (STEM) have been carried out to gather microstructural insights into the composite in a three-dimensional (3D) manner. The 2D micrographs acquired at different angles of tilt, as a part of the tomography experiment and slices redrawn from the 3D reconstructed volume of the composite zeolite, show the coexistence of two zeolites Y and ZSM-5 (Figure 8). These results are in good agreement with the high-resolution TEM images (Figures 6E and 6F), revealing the unique formation of nano-ZSM-5 zeolite in and around the USY by using only the nutrition (Si and Al) provided during the acid treatment of the USY. The 3D reconstruction images reveal that the center of the composite possesses an octahedral morphology typical of FAU zeolite (Figures 8D and S9), whereas the nano-ZSM-5 zeolite crystals grow predominantly on the periphery of the USY-A crystals. A particular feature distinguished in the slices of the reconstructed image is the presence of both mesopores and channels within the FAU zeolite crystals (Figures 8D and S9), which ensure the accessibility to the inner porous network. The channels and/or open mesopores within the FAU central zeolites appear to be filled by nano-ZSM-5 zeolites, leading to an increased surface area. The complex morphology of the composite, with the FAU zeolite embedded by nanosized ZSM-5 zeolites arranged in a rather continuous and porous structure shapes the hierarchical structure made of two types of micropores and mesopores.

Besides the mass transfer that generates the composite zeolite composed of hierarchical USY and nanosized ZSM-5, the redistribution of Si and Al elements during the transformation is another matter of interest. Herein, STEM-energy-dispersive X-ray spectroscopy (EDS) mapping (Figure 9) provides information on the Si/Al ratio of the composite sample. A representative STEM image showing the coexistence of both zeolites is shown in Figure 9A. The Si/Al ratios of the "zone 1" and "zone 2" determined by EDS are 13.9 and 26.5, respectively. This is expected considering that the Si/Al ratio of the USY-A zeolite is 22.7 and the interzeolite conversion treatment is essentially a combination of two

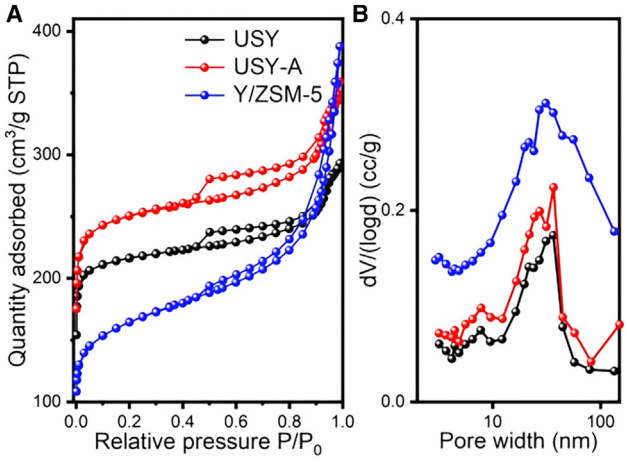

Figure 4. N_2 physisorption and mesopore analysis

N_2 physisorption isotherms (A) and the corresponding mesopore size distributions (B) derived from the adsorption branch of the parent USY, acid-treated USY-A zeolite, and Y/ZSM-5 composite. STP, standard temperature and pressure.

Please cite this article in press as: Zhang et al., Zeolite composite prepared by quasi-*in situ* interzeolite conversion approach, Chem Catalysis (2025), https://doi.org/10.1016/j.checat.2025.101298

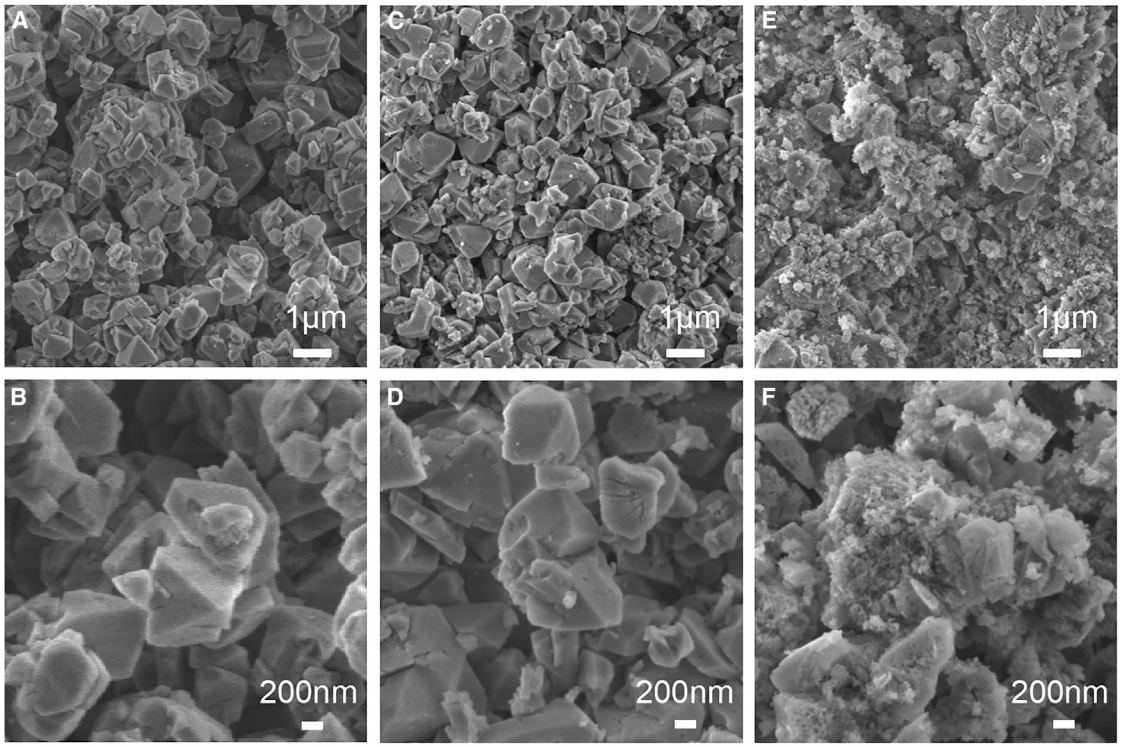

Figure 5. Morphology study of SEM images

SEM images of parent USY (A and B), acid-treated USY-A (C and D), and Y/ZSM-5 composite (E and F) at different magnifications. Scale bars: 1 μm (A, C, and E) and 200 nm (B, D, and F).

successive processes—desilication in the presence of OH^- and nucleation and crystallization of ZSM-5 mediated by TPA^+ and OH^-. While the preferential removal of framework Si atoms decreases the Si/Al ratio of the USY-A zeolite sample from 22.7 to 13.9 (zone 1), the growth of ZSM-5 zeolite templated by TPA^+ results in a product with a Si/Al ratio of no less than 24, as each unit cell of MFI-type zeolite can accommodate up to 4 TPA^+.[44]

FTIR

The samples were also subjected to Fourier transform infrared spectroscopy (FTIR) characterization. The FTIR spectra in the stretching region of the hydroxyl groups of the samples are depicted in Figure 10. The OH bands in the spectrum of USY appear with very low intensity in comparison to those measured for USY-A zeolite. The intensity of the band corresponding to isolated (3,745 cm^{-1}) and terminal (3,735 cm^{-1}) silanols increase approximately 82%; the calculation is based on the normalized area between 3,760 and 3,710 cm^{-1} related to the presence of four types of silanol groups.[45]

In the case of the composite material, another peak at 3,609 cm^{-1} appears in the hydroxyl region associated with the Brønsted sites of MFI-type zeolites.[46] The peak intensity between 3,650 and 3,600 cm^{-1} for Y/ZSM-5 increased 39% compared to USY-A. The acidity of the Y/ZSM-5 composite is significantly higher compared to USY-A zeolite (Figure 10B; Table 2). The increase in acidity is due to the high amount of ZSM-5 zeolite newly formed in the composite.[45–47] However, this increase in acidity is also caused by opening the SOD cages during the acid treatment of USY.[12] The appearance of this new peak at 3609 cm^{-1} and the increase in the total concentration of the acid sites further confirm the formation of an MFI-type zeolite in the Y/ZSM-5 composite. In addition, there is a decrease of approximately 38% in the silanol sites (semi-quantitative data calculated by evaluating the area of the peaks in the range 3,760–3,710 cm^{-1}). This can be attributed to the consumption of the hydroxyl sites from the USY and the formation of the ZSM-5 zeolite.

Furthermore, to evaluate the acidity and the accessibility of these acid sites, adsorption with 2,6-di-*tert*-butylpyridine (dTBPy) was performed (Table 2). dTBPy has a kinetic diameter (15.8 Å) larger than the pore sizes of both zeolites FAU and MFI.[48] At 150°C, approximately 12% of the acidic sites in USY were accessible to the basic probe dTBPy within 20 min (Table 2). In the case of the USY-A zeolite, the number of accessible acid sites increased considerably, up to 68%. In the Y/ZSM-5 composite, the accessibility of acidic sites increased to 83%. Although ZSM-5 zeolite has a smaller pore size than USY zeolite and the Y/ZSM-5 composite contains a large proportion of ZSM-5, the composite exhibits more external acid sites and higher accessibility. This is attributed to the defects exposed by the dissolution of USY zeolite and the high specific surface area of ultra-small nano-ZSM-5.

Hyperpolarized ^{129}Xe NMR

Hyperpolarized (HP) ^{129}Xe NMR was further applied to characterize the pore connectivity between USY and ZSM-5 zeolites

Please cite this article in press as: Zhang et al., Zeolite composite prepared by quasi-*in situ* interzeolite conversion approach, Chem Catalysis (2025), https://doi.org/10.1016/j.checat.2025.101298

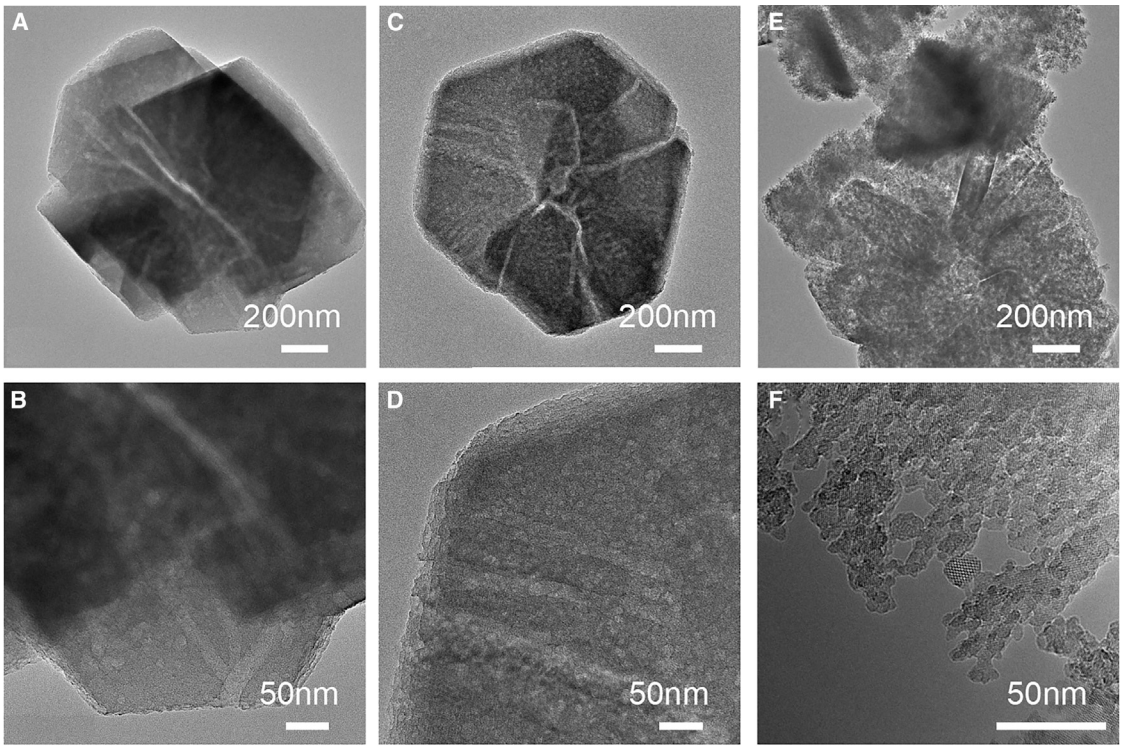

Figure 6. Morphology and porosity properties study of TEM images

TEM images of parent USY (A and B), acid-treated USY-A (C and D), and Y/ZSM-5 composite (E and F) at different magnifications. Scale bars: 200 nm (A, C, and E) and 50 nm (B, D, and F).

in the composite (Figure 11). As a reference, a mixture was prepared by mixing the USY-A zeolite and nanosized ZSM-5 zeolite (supplemental methods) with the same ratio as in the composite Y/ZSM-5. The temperature-dependent HP ^{129}Xe NMR spectra are presented in Figure S10. The broad peaks at 193 K are attributed to the Xe molecule accommodated in the FAU structure originating from the formation of open SOD cages and mesopores.[13] The peaks at the higher chemical shift are attributed to the Xe molecule located in the MFI pores.[49] Due to the rapid exchange of Xe between different pores and the reduced adsorption capacity at high temperatures, the low-intensity peaks are difficult to assign straightforward. By comparing the spectra of the Y/ZSM-5 composite and the mechanical mixture (MM; reference sample) collected at 173 K (Figure 11), one can observe faster Xe exchange between the two pore systems of the composite containing intergrown USY and ZSM-5 zeolites, representing better pore connectivity.

Catalytic reaction: MTO reaction and cracking of n-hexane

The three samples USY, USY-A, and Y/ZSM-5 were further evaluated in the methanol-to-olefins (MTO) reaction. The methanol (MeOH) and dimethylether (DME) conversion over the different catalysts as a function of the reaction time is presented in Figure 12A. The selectivity toward methane (CH_4), ethene (C_2=), propene (C_3=), butenes (C_4=), butane (C_4), pentenes plus pentane (C_5), and aliphatics plus aromatics (C_6^+) at different MeOH and DME conversion levels and various reaction durations is presented in Figures 12B–12D): 100% at initial time (Figure 12B), 100% before deactivation (Figure 12C), and between 12% and 19%, respectively. Finally, the latter conversion was also expressed at different reaction times (Figure 12D).

Catalyst lifetime, stability, and selectivity depend on several parameters, including pore structure (cage size and shape, pore openings) and acid site strength and density.[50] As shown, the three catalysts exhibit different behaviors in terms of stability and selectivity toward products throughout the reaction. The catalysts led all to the same initial full conversion. After less than 2 h, substantial deactivation occurs in the case of USY and USY-A zeolites. In contrast, Y/ZSM-5 composite remains stable for more than 10 h, thus suffering slower deactivation. At the start of the reaction, interestingly, product selectivity remained the same regardless of the zeolite structure. In the case of USY and USY-A zeolite catalysts, methane selectivity increases steadily during the reaction, contrary to Y/ZSM-5. Since the MTO reaction is governed both by the activity of the Brønsted acid site (BAS) and by a hydrocarbon pool mechanism,[51,52] numerous descriptors such as methane, ethene, and propene can be used to understand the different catalytic behaviors.[53,54] Methane represents the hydrogen-rich co-product of the formation of hydrogen-deficient coke molecules and can be formed by the dehydrogenation of coke molecules with methanol. Ethene is mainly formed from aromatics, especially polymethylbenzenes, by successive methylation and dealkylation reactions

Please cite this article in press as: Zhang et al., Zeolite composite prepared by quasi-*in situ* interzeolite conversion approach, Chem Catalysis (2025), https://doi.org/10.1016/j.checat.2025.101298

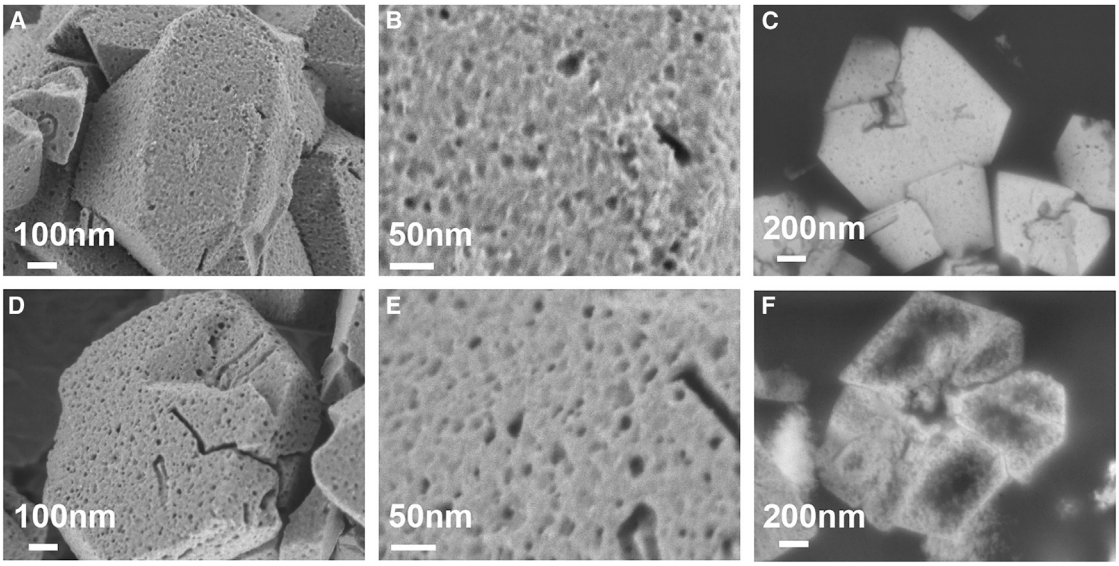

Figure 7. Surface and internal porosity study

High-resolution SEM images and cross-section SEM images of zeolite USY (A–C) and the Y/ZSM-5 composite (D–F) at different magnifications. Scale bars: 100 nm (A and D), 50 nm (B and E), and 200 nm (C and F).

(aromatic-based cycle).[51] Concerning propene, it is mainly formed from long-chain alkenes by methylation and oligomerization reactions followed by β-scission (alkene-based cycle).[55] The ethene/propene ratio can be used to investigate the relative contribution of each cycle during the reaction.

For the USY catalyst, the selectivity toward methane increases with the decrease in methanol conversion and selectivity toward C_6^+ products. The reaction begins with the predominance of the alkene-based cycle, with an ethene/propene ratio of 0.37, which gradually gives way to a greater relative contribution to the aromatic-based cycle, with a ratio of 1.68 before deactivation and before ending at low conversion with a ratio of 0.35. This rapid deactivation is due to a very fast coke deposition, reaching 22 wt. % after 2 h of reaction (Figure S11). This deactivation can be related to the BAS density of the USY zeolite and the large pores inside the structure. Easier diffusion of aromatic species leading to acid-catalyzed consecutive reactions can be assumed. The coke precursor species retained in the zeolite structure could react with methanol, resulting in a dominant dehydrogenation reaction with methane as a hydrogen-rich co-product. At the end of the reaction, methane remains the most relevant deactivation descriptor to use, with a selectivity of 90%, as shown in Figure 12D. This indicates a mechanism governed predominantly by the growth of coke molecules. The same deactivation mechanism for FAU zeolite has been reported previously.[56–58]

For USY-A, the results indicate the same lifetime but a different behavior in terms of selectivity and coke content, which is lower after dealumination (15 wt. %; Figure S11). At the beginning of

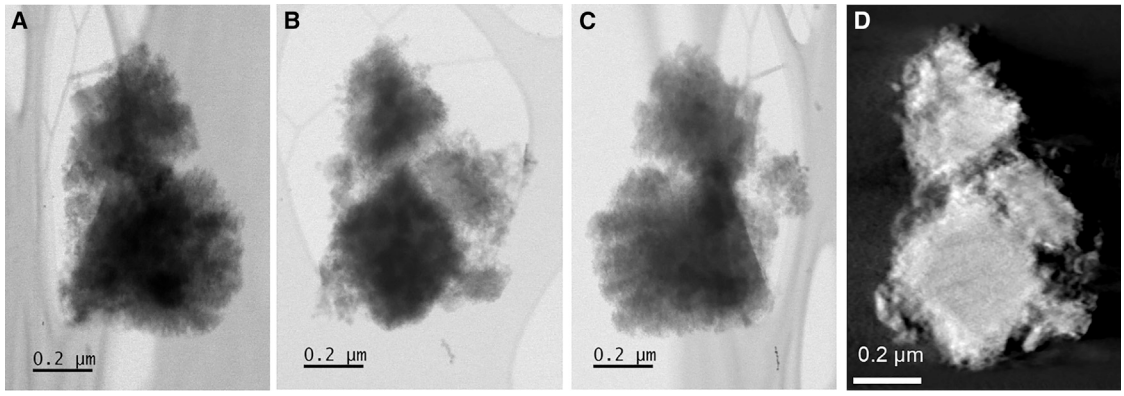

Figure 8. STEM images and 3D reconstructed image

STEM images and 3D reconstructed images: STEM-BF images tilt +72° (A), 0° (B), and −72° (C). Slice redrawn from the STEM-HAADF reconstructed volume along a random direction (D).

Please cite this article in press as: Zhang et al., Zeolite composite prepared by quasi-*in situ* interzeolite conversion approach, Chem Catalysis (2025), https://doi.org/10.1016/j.checat.2025.101298

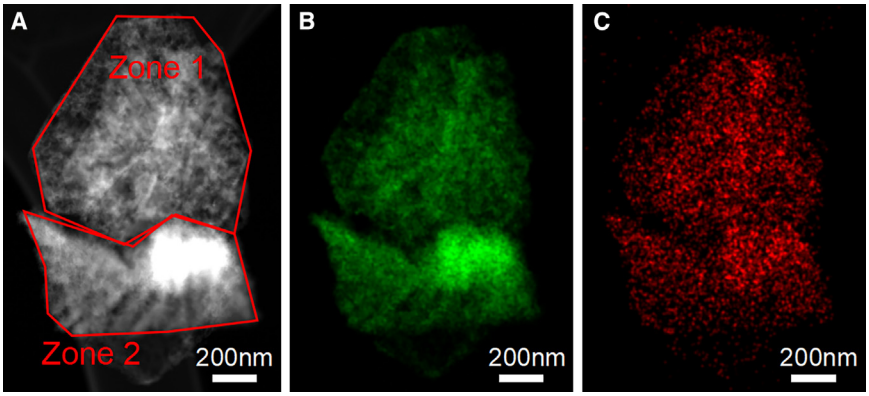

Figure 9. Changes in Si and Al elements of composite zeolite from EDS data
STEM image of the Y/ZSM-5 composite (A), and the corresponding EDS mapping images showing the Si (B) and Al (C) element distribution.

the reaction, propene is the main product formed. The reaction then evolves toward the subsequent formation of methane and ethene. These results indicate a change in the reaction mechanism from the alkene-based cycle to the aromatic-based cycle during the reaction. This can be confirmed by a change in the ethene/propene ratios from 0.32 at 100% of conversion at the initial time and before deactivation to 3.62 at 12% of conversion at the end of the reaction (Figures 12B and 12D). Apparently, dealumination of the structure changed the selectivity in the products despite a similar lifetime, and pore-blocking deactivation mode to the pristine USY is observed. The applied dealumination results in a 16% increase in micropore volume and a 43% increase in mesopore volume, besides a 76% decrease in the total amount of acidity (Tables 1 and 2). Several studies have shown that propene formation is favored by a lower density of BAS, potentially inducing better spacing between each site, and the presence of mesopores allowing easier access to the active sites for reagents and better diffusion and internal porosity exit of the products.[28,59]

The Y/ZSM-5 composite catalyst, consisting of 40% USY-A and 60% ZSM-5, demonstrates a longer catalyst lifetime and better resistance to coking, with only 12 wt. % coke formed after 25 h of reaction (Figure S11). Propene formation remains the main product throughout the reaction, indicating a strong relative contribution from the alkene-based cycle. This is supported by the constant ethene/propene ratios of 0.27, 0.17, and 0.29 at the initial time, before deactivation at 100% of conversion, and 19% of conversion. These results are similar to those obtained with a pure ZSM-5 zeolite.[60–62] However, this does not mean that all active sites are located within the ZSM-5 pores because nearly the same selectivity toward products was obtained with both USY catalysts at the initial reaction time of 0.08 h, as shown in Figure 12B. However, a relationship can be established between the shape-selective structure of ZSM-5, which promotes access to the active sites only by low-hindrance molecules, and the prominent participation of the alkene-based cycle maintained throughout the reaction. Additionally, the selectivity of C_6^+ products increases as the reaction proceeds, with the ethene/propene ratio below 1 during the entire reaction. This may be due to secondary reactions whose larger molecules are able to exit thanks to the larger pores of the Y zeolite. In this case, the Y/ZSM-5 composite shows improved stability, with a protective effect originating from the presence of nano-sized ZSM-5 crystals on the mesoporous Y zeolite. Finally, the confinement effect within ZSM-5 micropores in the composite makes it possible to control the size of the molecules formed during the reaction.[63,64] Deactivation therefore appears slower and the catalyst avoids sudden deactivation with instantaneous blocking by pore filling. To complete these data, an MM was made with the commercial USY and a nano-ZSM-5 zeolite in the same mass proportions as the composite (see methods section). The results obtained show that the catalytic behavior of the MM is like that of the composite—in other words, same lifetime, same selectivity toward the products, and same ethene/propene ratio over the reaction time. The MM contained 18 wt. % coke after the catalytic test, which is 1.5 times more than that of the composite. Given that ZSM-5 rarely exceeds 10 wt. % coke content, it is possible that some of the coke from the MM was trapped in the USY zeolite.[65]

To further study the catalytic behavior, the samples were evaluated in the n-hexane cracking reaction, performed at 540°C under atmospheric pressure. Catalyst activity was determined from the slope of the first-order rate equation. The turnover frequency (TOF) and paraffin-to-olefin (p/o) ratios for the different materials are presented in Table 3. The TOF was calculated by normalizing the activity to the number of BASs capable of retaining pyridine at 150°C.

Notably, no deactivation was observed, confirming that the operating conditions were ideal for the monomolecular cracking mechanism to dominate. Acid leaching generated EFAL species, which enhanced the activity of the BAS, leading to an increased TOF for USY-A.[66,67] However, when EFAL species recrystallized within the ZSM-5 framework to form the composites, this enhancement effect disappeared, resulting in a decreased TOF for the Y/ZSM-5 composite. Due to their similar acidity, the TOF of the composite was comparable to that of the corresponding MM, with a slight increase.

The p/o ratio provides a straightforward measure of the contributions of primary and secondary cracking reactions. When the p/o ratio equals 1, only primary cracking occurs; ratios less than 1 indicate secondary cracking.[68] The composite material exhibited a significant increase in the p/o ratio compared to the MM, suggesting that the close interaction between Y and ZSM-5 crystals facilitated olefin desorption and diffusion, thereby reducing secondary cracking.

Conclusion

The present work reports a quasi-*in situ* interzeolite conversion approach for the synthesis of Y/ZSM-5 composite with upgraded mesoporosity and pore connectivity. The interzeolite

Please cite this article in press as: Zhang et al., Zeolite composite prepared by quasi-*in situ* interzeolite conversion approach, Chem Catalysis (2025), https://doi.org/10.1016/j.checat.2025.101298

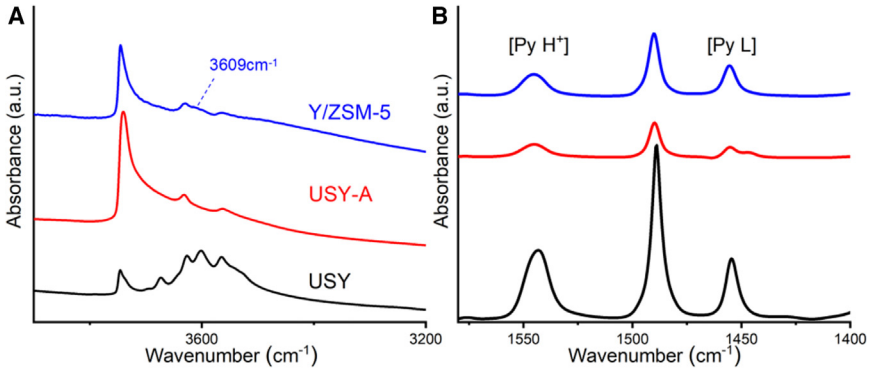

Figure 10. Hydroxyl groups changes and acidity study from FTIR

FTIR spectra in the stretching region of the hydroxyl groups (3,900–3,200 cm^{-1}) (A) and after adsorption of Py (1,560–1,400 cm^{-1}) (B) of parent USY, acid-treated USY-A zeolite, and Y/ZSM-5 composite.

conversion was achieved through the partial removal of atoms from the USY framework and the subsequent conversion of the dissolved species (Al and Si) into ZSM-5 zeolite in the presence of TPAOH, which serves as a part of the alkaline leaching of the USY zeolite framework and as the template for the growth of ZSM-5 zeolite. Thanks to the restricted dissolution and confined mass transfer in the quasi-solid-state interzeolite conversion system, the composite consists of a hierarchical USY zeolite with a highly mesoporous network and a nanosized ZSM-5 zeolite. The high mesopore volume, homogeneous distribution of mesopores, and the intimate pore connectivity of the two zeolites in the composite are comprehensively characterized by FTIR-pyridine, dTBPy, and and HP ^{129}Xe NMR. In the MTO reaction, the composite shows an alkene-based cycle-dominated product distribution and a delayed deactivation behavior, indicating the positive effect of the composite consisting of intergrown USY and ZSM-5 zeolites. The relative concentration of the two zeolites in the composite can be tuned through an adjustment of the Si/Al ratio of the parent USY zeolite, and thus we envisage the interzeolite conversion as a potential route to be applied broadly for the preparation of hierarchical composite important for catalysis and adsorption.

METHODS

Materials

A commercial USY zeolite with a bulk Si/Al ratio of 6.1, purchased from Qilu Huaxin High-Tech, was used as the raw material. The sulfuric acid (98%), ammonium sulfate (99.0%), and TPAOH (25 wt. % aqueous solution) were purchased from Sinopharm Chemical Reagent Corporation. Deionized water was homemade, using an ultra-pure water purification system (PINE-TREE, XYF2-10-H).

Table 2. Acidity of samples measured by FTIR using pyridine and dTBPy probe molecules

	Pyridine, μmol/g		dTBPy, μmol/g	Acid accessibility
Sample	BASs, 1,540 cm^{-1}	LASs, 1,450 cm^{-1}	BASs, 3,360 cm^{-1}	BAS_{dTBPy}/BAS_{Py}, %
USY	547	188	67	12
USY-A	115	58	79	68
Y/ZSM-5	148	104	123	83

Synthesis of Y/ZSM-5 composite

Dealumination of USY zeolite by acid leaching

In a typical procedure, 70 g aqueous sulfuric acid solution (10 wt. %) was mixed with 10 g ammonium sulfate and 100 g deionized water to make a homogeneous solution. Then, 10 g of the commercial USY zeolite was added to the solution. The temperature of the resultant suspension was increased to 358 K and kept at this temperature for 2 h. After that, the solid was collected by vacuum filtration, washed thoroughly with deionized water, and dried at 373 K overnight. The sample, denoted as USY-A, was recovered and used for the subsequent interzeolite conversion.

Y/ZSM-5 composite prepared by quasi-in situ interzeolite conversion

For the preparation of the Y/ZSM-5 composite, the USY-A zeolite was impregnated with the TPAOH solution first. In a typical experiment, 0.8 mL of the 25 wt. % TPAOH solution was added dropwise to 1 g of the USY-A, with intermittent mixing using a spatula. The impregnated zeolite was then placed in a Teflon-lined stainless-steel autoclave and heated in an oven for 12 h at 393 K and then for 24 h at 413 K. The final zeolite composite was recovered by centrifugation, washed thoroughly with deionized water, and dried at 373 K overnight. The obtained composite was designated as Y/ZSM-5. The H-form of this sample was derived by calcination at 823 K for 6 h with a heating ramp of 2 K/min starting from room temperature.

Materials characterization

XRD patterns of samples were recorded using a powder X-ray diffractometer (Bruker D8 Advance) with Cu-Kα radiation at 30 mA and 40 kV; the XRD standard spectra of Y and ZSM-5 zeolite from the Bruker AXS database were used as references. The phase ratios of the zeolites in the composite zeolite estimated are presented in the supplemental methods. An AXIOS-Petro X-ray fluorescence spectrometer (PANalytical B.V.) was used to determine the bulk Si/Al ratio of the samples. Nitrogen physisorption analysis at 77 K was performed using an Autosorb iQ3 (Quantachrome) gas adsorption analyzer. Samples were degassed at 573 K for 6 h prior to analysis. The specific surface areas of the samples were determined using the Brunauer-Emmett-Teller (BET) equation. The *t* plot method was used to distinguish the contribution from micropores and mesopores.

SEM images were taken with a JSM-7900F (JEOL) electron microscope equipped with a field emission gun. An ion beam cross-section polisher (IB-19510CP, JEOL) was used for the preparation of the cross-section of the zeolite samples. The zeolite crystals were immobilized on a carbon tape prior to

Please cite this article in press as: Zhang et al., Zeolite composite prepared by quasi-*in situ* interzeolite conversion approach, Chem Catalysis (2025), https://doi.org/10.1016/j.checat.2025.101298

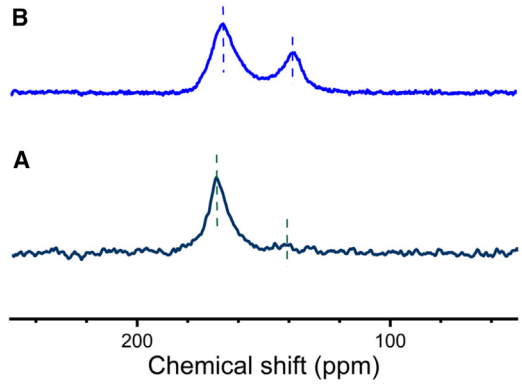

Figure 11. Channel connectivity characterized by HP ^{129}Xe NMR
HP ^{129}Xe NMR spectra recorded at 173 K for the mechanical mixture (reference sample) prepared from USY-A and nanosized ZSM-5 zeolite (A) and the Y/ZSM-5 composite (B).

the preparation of the cross-sections. The high-resolution images and cross-section images were collected with a JSM-IT800 scanning electron microscope. TEM images were taken on a JEM-2100 (JEOL) with an accelerating voltage of 200 kV. STEM images were acquired on a JEOL JEM-F200 electron microscope with a Gatan Rio 1816 (IS) camera, allowing a point resolution of 1.9 Å under STEM mode, equipped with a JEOL SDD EDS detector (100 mm 2 × 1). All STEM images and EDS spectra were recorded at a 200-kV acceleration voltage.

The electron tomography (ET) investigations were carried out at 80 kV to avoid the specimen damage upon long-duration exposure to the electron beam. For the ET series acquisition, the specimen was tilted from −78° to +75° with a step of 2° and following the equal angle tilting schema implemented in Digital Micrograph software. The 1,024 × 1,024-pixel bright-field (BF) and high-angle annular dark-field (HAADF) STEM micrographs were simultaneously acquired at a scanning speed of 10 μs/pixel. The image alignments were carried out by cross-correlation followed by manual alignment using gold nanoparticles as fiducial markers, as implemented in ETomo software. Afterward, the volume reconstruction was performed in ImageJ using the TomoJ plugin and the OS-ART iterative algorithms for 20 iterations. The volume visualization and rendering was performed in Fiji (ImageJ).

The HP ^{129}Xe NMR spectra were recorded on a Bruker Avance III 500 MHz (11.7 T) spectrometer with a continuous-flow HP Xe delivery apparatus. The materials were transferred into a 10-mm quartz tube in an Ar glove box after being dehydrated under vacuum for 10 h at 693 K prior to the NMR study. With a 120-Gs optical pumping cell and a 120-W diode laser array (Coherent fiber array package system), HP ^{129}Xe was produced. At a rate of 200 mL/min, the gas mixture of 1% Xe, 1% N_2, and 98% He was introduced to the quartz NMR tube (10 mm). The resonance frequency of ^{129}Xe was 110.7 MHz. A single pulse sequence with a pulse width of 18 s under 50 W pulse power, a recycle delay of 2 s, and 128 times scan was used to accumulate 1D HP ^{129}Xe NMR spectra. The temperature ranged from 298 to 173 K during the trials, with variable temperature. All the ^{27}Al and ^{29}Si MAS NMR spectra were recorded on a Bruker Advance 500 MHz spectrometer using a 4-mm rotor. The ^{27}Al MAS NMR spectra were recorded at 104.3 MHz with a 12-pulse length of 2.2 s, a spinning rate of 14 kHz, and a recycle delay of 1 s. For chemical shifts of ^{27}Al MAS NMR spectra, 1 M $Al(NO_3)_3$ was used as a reference.

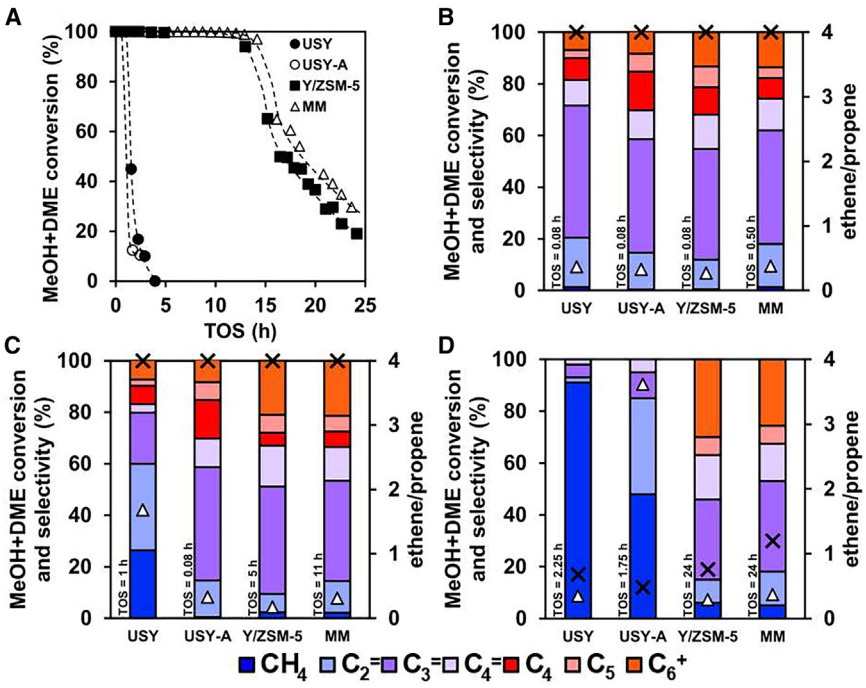

Figure 12. The methanol-to-olefin reaction
MeOH and DME conversion over time-on-stream (TOS), cumulative product selectivity, and ethene/propene ratio (A) at 100% conversion of MeOH and DME at the initial time (B), 100% conversion before deactivation (C), and 12%–30% iso-conversion deactivation conditions (D). The white triangles and black crosses correspond to ethene/propene ratios and conversions on product selectivity, respectively.

Please cite this article in press as: Zhang et al., Zeolite composite prepared by quasi-*in situ* interzeolite conversion approach, Chem Catalysis (2025), https://doi.org/10.1016/j.checat.2025.101298

Table 3. TOF and p/o ratios of parent USY zeolite, acid-treated USY-A zeolite, Y/ZSM-5 composite, and MM corresponding to the equivalent amount of acid with Y/ZSM-5 composite

Sample	TOF, h^{-1}	p/o ratio
USY	46	0.42
USY-A	288	0.69
Y/ZSM-5	171	0.69
MM	182	0.55

IR spectra were recorded using a Nicolet Magna 550-FTIR spectrometer at 4 cm^{-1} optical resolution and 64 scans. The zeolite powder was pressed into a self-supporting disc (1.6 cm in diameter, ~20 mg) and pretreated in the *in situ* IR cell under vacuum at 723 K (2 K min^{-1}) for 4 h under 10^{-6} Torr. The adsorption of pyridine was performed at 423 K at 1 Torr pyridine to reach equilibrium. Then, the cell was evacuated at 373–673 K. The amount of pyridine that remained adsorbed after the evacuation was determined using the integrated area of the IR bands at 1,545 and 1,454 cm^{-1} corresponding to BAS and Lewis acid site (LAS), respectively. The extinction coefficients used for pyridine were $\varepsilon(B)_{1,545}$ = 1.36 cm/μmol, and $\varepsilon(L)_{1,450}$ = 1.5 cm/μmol for BAS and LAS, respectively. The adsorption of dTBPy was performed at 423K with excess of dTBPy probe molecules. Then, the cell was evacuated at the same temperature and followed by collection of the spectrum at room temperature. The amount of dTBPy was determined using the integrated area of the bands at 3,360 cm^{-1}. All spectra were normalized to the density of a wafer.

Catalytic test

MM preparation

A reference MM was made from commercial nano-ZSM-5 (Si/Al = 43, the information reported by Beuque et al.[69]) and USY zeolite (Si/Al = 6.1, raw material). This MM was composed to have Si/Al ratio and Y/ZSM-5 phase ratio characteristics similar to those of the composite.

MTO

The MTO reaction was performed on the samples in a fixed-bed reactor at an atmospheric pressure of 723 K. Catalyst, 0.1 g, with a particle size in the range of 0.2–0.4 mm was packed in a quartz tube reactor (7 mm internal diameter). Prior to the reaction, the catalyst was pre-treated under heating room temperature of 823 K with a heating rate of 5 K min^{-1} under a nitrogen flow of 55 mL min^{-1} for 1 h. Then, it was cooled to the reaction temperature. The MTO reaction was carried out at a weight hourly space velocity (WHSV) of 2.1 g MeOH g_{cat}^{-1} h^{-1}, with a continuous flow of nitrogen (55 mL min^{-1}) and liquid methanol (MeOH) (0.0044 mL min^{-1}) instantaneously vaporized at the reactor inlet. The gas composition at the reactor outlet was characterized by online gas chromatography (Chromatec, Crystal 9000) equipped with a flame ionization detector (FID; PONA column). Conversion and selectivity have been calculated according to Equations 1 and 2, respectively:

$$X_{MeOH+DME}(\%)\frac{A_{Tot}^{outlet} - A_{MeOH}^{outlet} - 2A_{DME}^{outlet}}{A_{Tot}^{outlet}} \quad \text{(Equation 1)}$$

where A_{Tot}^{outlet} is the area of total product peaks in the reactor outlet, A_{MeOH}^{outlet} is the area of the MeOH peak measured at a given time in the reactor outlet, and A_{DME}^{outlet} is the area of the DME peak measured at a given time in the reactor outlet.

$$S_i(wt.\%) = \frac{Y_i^{outlet}}{X_{MeOH+DME}} \times 100 \quad \text{(Equation 2)}$$

where Y_i^{outlet} is the product mass yield.

C, H, N elemental analysis was carried out using Thermo Fisher Scientific Flash 2000 for coke nature and total carbon percentage of the spent catalysts.

n-Hexane cracking

The transformation of n-hexane, chosen as the model reaction, is carried out on throughput four-parallel fixed-bed reactors unit. To have an accurate estimation of the reaction rate, the reaction is carried out at four contact times by using different amounts of the same catalyst, with a particle size of 0.2–0.4 mm in each reactor (20, 40, 60, and 80 mg) and pre-treated at 540°C under nitrogen flow for 12 h. Diluted n-hexane (99.99% pure from Sigma-Aldrich) in nitrogen flow was then injected in the reactors at 540°C, with a molar ratio of 11 ($P_{N2}/P_{n\text{-hexane}}$ = 11). Catalyst activity is measured by estimating the conversion at different values of the WHSV. Reaction products of each reactor were analyzed by online gas chromatography equipped with a Cp-Al_2O_3/Na_2SO_4 capillary column (50 m, 10 μm) coupled with an FID.

The activity per BAS expressed by the TOF (h^{-1}), was calculated as follows:

$$TOF = \frac{A_0}{[PyH^+] \times M_{n-hex}}$$

where A_0 (μmol/h/g_{cat}) is the initial catalyst activity estimated graphically by the initial slope of the plot $-Ln(1 - X)$ vs. 1/WHSV (X is the conversion), $[PyH^+]$ is the concentration of BASs of the catalyst determined after pyridine desorption at 150°C (μmol/g_{cat}), and M_{n-hex} is the molar weight of the n-hexane (g/mol).

RESOURCE AVAILABILITY

Lead contact

Further information and requests for resources and reagents should be directed to and will be fulfilled by the lead contact, Svetlana Mintova (svetlana.mintova@ensicaen.fr).

Materials availability

This study did not generate new materials.

Data and code availability

This study did not generate any datasets.

ACKNOWLEDGMENTS

Z.Q. acknowledges support from NSFC 22178389. S. Mintova acknowledges support from NSFC 21975285. Z.Q. and S. Mintova acknowledge support from NSFC 21991090 and NSFC21991091 and PetroChina (PRIKY21084 and KYWX-21-021). S. Mintova was cofunded by the European Union (ERC, ZEOLIghT, 101054004). L.P. thanks the European Union's Horizon 2020 research and innovation program for its funding under grant agreement no. 814548. C.L., B.L., and L.P. acknowledge financial support from SATT

Conectus and "Région Normandie." C.L. and L.P. thank the Région Normandie for funding the BioDNH "Chaire d' Excellence." GENESIS is supported by the Région Haute-Normandie, the Métropole Rouen Normandie, the CNRS via LABEX EMC, and the French National Research Agency as a part of the program "Investissements d'avenir" with the reference no. ANR-11-EQPX-0020. This work was partially supported by the CNRS federation IRMA - FR 3095. The views and opinions expressed in this paper are those of the author(s) only and do not necessarily reflect those of the European Union or the European Research Council. Neither the European Union nor the granting authority can be held responsible for them.

AUTHOR CONTRIBUTIONS

S. Mintova, Z.Q., and X.G. conceived and supervised the project. R.Z. and B.W. performed the primary experimental synthesis steps, including preliminary experimental exploration and basic characterizations such as XRD, SEM, and TEM. H.L., H.Z., and J.W. participated in the synthesis, characterization, and verification of the concept. R.Z. carried out the ^{29}Si and ^{27}Al NMR analysis and the adsorption characterizations. J.X. and S.X. conducted the HP ^{129}Xe NMR analysis. S.A. performed the high-resolution SEM and cross-section SEM characterizations. S. Moldovan conducted the STEM imaging and the 3D reconstruction analysis. F.D. and R.Z. collected and analyzed the FTIR data. C.L., B.L., and L.P. carried out the MTO reaction and the n-hexane cracking experiments. Z.Q., R.Z., F.D., and L.P. drafted the manuscript. All authors contributed to discussions and revisions of the paper.

DECLARATION OF INTERESTS

Z.Q. is listed as an author on Chinese patent CN 201811455884.4 (2020), and Z.Q. and H.L. are listed as authors on Chinese patent application 202311499444X (2023).

SUPPLEMENTAL INFORMATION

Supplemental information can be found online at https://doi.org/10.1016/j.checat.2025.101298.

Received: September 23, 2024
Revised: October 30, 2024
Accepted: January 31, 2025
Published: March 4, 2025

REFERENCES

1. Davis, M.E. (2002). Ordered porous materials for emerging applications. Nature *417*, 813–821. https://doi.org/10.1038/nature00785.
2. Martínez, C., and Corma, A. (2011). Inorganic molecular sieves: Preparation, modification and industrial application in catalytic processes. Coord. Chem. Rev. *255*, 1558–1580. https://doi.org/10.1016/j.ccr.2011.03.014.
3. Mintova, S., Gilson, J.P., and Valtchev, V. (2013). Advances in nanosized zeolites. Nanoscale *5*, 6693–6703. https://doi.org/10.1039/c3nr01629c.
4. Shi, J., Wang, Y., Yang, W., Tang, Y., and Xie, Z. (2015). Recent advances of pore system construction in zeolite-catalyzed chemical industry processes. Chem. Soc. Rev. *44*, 8877–8903. https://doi.org/10.1039/c5cs00626k.
5. Lang, Q., Lu, P., Yang, X., and Valtchev, V. (2024). Zeolites for the environment. Green Carbon *2*, 12–32. https://doi.org/10.1016/j.greenca.2024.02.007.
6. Wu, Q., Wang, X., Qi, G., Guo, Q., Pan, S., Meng, X., Xu, J., Deng, F., Fan, F., Feng, Z., et al. (2014). Sustainable synthesis of zeolites without addition of both organotemplates and solvents. J. Am. Chem. Soc. *136*, 4019–4025. https://doi.org/10.1021/ja500098j.
7. Li, Y., Li, L., and Yu, J. (2017). Applications of zeolites in sustainable chemistry. Chem. Soc. Rev. *3*, 928–949. https://doi.org/10.1016/j.chempr.2017.10.009.
8. Mallette, A.J., Seo, S., and Rimer, J.D. (2022). Synthesis strategies and design principles for nanosized and hierarchical zeolites. Nat. Synth. *1*, 521–534. https://doi.org/10.1038/s44160-022-00091-8.
9. Serrano, D.P., Centi, G., Diddams, P.A., and Čejka, J. (2024). Outlooks for zeolite catalysts in a low-carbon scenario. Catal. Today *426*, 114365. https://doi.org/10.1016/j.cattod.2023.114365.
10. Xia, Y., Cao, H., Xu, F., Chen, Y., Xia, Y., Zhang, D., Dai, L., Qu, K., Lian, C., Huang, K., et al. (2022). Polymeric membranes with aligned zeolite nanosheets for sustainable energy storage. Nat. Sustain. *5*, 1080–1091. https://doi.org/10.1038/s41893-022-00974-w.
11. Li, J., Gao, Z.R., Lin, Q.F., Liu, C., Gao, F., Lin, C., Zhang, S., Deng, H., Mayoral, A., Fan, W., et al. (2023). A 3D extra-large-pore zeolite enabled by 1D-to-3D topotactic condensation of a chain silicate. Science *379*, 283–287. https://doi.org/10.1126/science.ade1771.
12. Qin, Z., Cychosz, K.A., Melinte, G., El Siblani, H., Gilson, J.P., Thommes, M., Fernandez, C., Mintova, S., Ersen, O., and Valtchev, V. (2017). Opening the Cages of Faujasite-Type Zeolite. J. Am. Chem. Soc. *139*, 17273–17276. https://doi.org/10.1021/jacs.7b10316.
13. Qin, Z., Zeng, S., Melinte, G., Bučko, T., Badawi, M., Shen, Y., Gilson, J.P., Ersen, O., Wei, Y., Liu, Z., et al. (2021). Understanding the Fundamentals of Microporosity Upgrading in Zeolites: Increasing Diffusion and Catalytic Performances. Adv. Sci. *8*, e2100001. https://doi.org/10.1002/advs.202100001.
14. Losch, P., Boltz, M., Bernardon, C., Louis, B., Palčić, A., and Valtchev, V. (2016). Impact of external surface passivation of nano-ZSM-5 zeolites in the methanol-to-olefins reaction. Appl. Catal. Gen. *509*, 30–37. https://doi.org/10.1016/j.apcata.2015.09.037.
15. Yusran, Y., Li, H., Guan, X., Li, D., Tang, L., Xue, M., Zhuang, Z., Yan, Y., Valtchev, V., Qiu, S., and Fang, Q. (2020). Exfoliated Mesoporous 2D Covalent Organic Frameworks for High-Rate Electrochemical Double-Layer Capacitors. Adv. Mater. *32*, e1907289. https://doi.org/10.1002/adma.201907289.
16. Zhou, W., Kang, J., Cheng, K., He, S., Shi, J., Zhou, C., Zhang, Q., Chen, J., Peng, L., Chen, M., and Wang, Y. (2018). Direct Conversion of Syngas into Methyl Acetate, Ethanol, and Ethylene by Relay Catalysis via the Intermediate Dimethyl Ether. Angew. Chem. *57*, 12012–12016. https://doi.org/10.1002/anie.201807113.
17. Vogt, E.T.C., and Weckhuysen, B.M. (2015). Fluid catalytic cracking: recent developments on the grand old lady of zeolite catalysis. Chem. Soc. Rev. *44*, 7342–7370. https://doi.org/10.1039/c5cs00376h.
18. Mirshafiee, F., Khoshbin, R., and Karimzadeh, R. (2022). A green approach for template free synthesis of Beta zeolite incorporated in ZSM-5 zeolite to enhance catalytic activity in MTG reaction: Effect of seed nature and temperature. J. Clean. Prod. *361*, 132159. https://doi.org/10.1016/j.jclepro.2022.132159.
19. den Hollander, M.A., Wissink, M., Makkee, M., and Moulijn, J. (2002). Gasoline conversion: reactivity towards cracking with equilibrated FCC and ZSM-5 catalysts. Appl. Catal. Gen. *223*, 85–102. https://doi.org/10.1016/S0926-860X(01)00745-1.
20. Ishihara, A. (2019). Preparation and reactivity of hierarchical catalysts in catalytic cracking. Fuel Process. Technol. *194*, 106116. https://doi.org/10.1016/j.fuproc.2019.05.039.
21. Milina, M., Mitchell, S., Crivelli, P., Cooke, D., and Pérez-Ramírez, J. (2014). Mesopore quality determines the lifetime of hierarchically structured zeolite catalysts. Nat. Commun. *5*, 3922. https://doi.org/10.1038/ncomms4922.
22. Smirniotis, P.G., Davydov, L., and Ruckenstein, E. (1999). Composite zeolite-based catalysts and sorbents. Catal. Rev. *41*, 43–113. https://doi.org/10.1081/CR-100101949.
23. Bouizi, Y., Diaz, I., Rouleau, L., and Valtchev, V.P. (2005). Core–shell zeolite microcomposites. Adv. Funct. Mater. *15*, 1955–1960. https://doi.org/10.1002/adfm.200500231.

24. Zornoza, B., Seoane, B., Zamaro, J.M., Téllez, C., and Coronas, J. (2011). Combination of MOFs and zeolites for mixed-matrix membranes. ChemPhysChem *12*, 2781–2785. https://doi.org/10.1002/cphc.201100583.

25. Moliner, M., Martínez, C., and Corma, A. (2015). Multipore zeolites: synthesis and catalytic applications. Angew. Chem. *54*, 3560–3579. https://doi.org/10.1002/anie.201406344.

26. Hosseinpour, N., Mortazavi, Y., Bazyari, A., and Khodadadi, A.A. (2009). Synergetic effects of Y-zeolite and amorphous silica-alumina as main FCC catalyst components on triisopropylbenzene cracking and coke formation. Fuel Process. Technol. *90*, 171–179. https://doi.org/10.1016/j.fuproc.2008.08.013.

27. Bazyari, A., Khodadadi, A., Hosseinpour, N., and Mortazavi, Y. (2009). Effects of steaming-made changes in physicochemical properties of Y-zeolite on cracking of bulky 1, 3, 5-triisopropylbenzene and coke formation. Fuel Process. Technol. *90*, 1226–1233. https://doi.org/10.1016/j.fuproc.2009.06.002.

28. Alotibi, M.F., Alshammari, B.A., Alotaibi, M.H., Alotaibi, F.M., Alshihri, S., Navarro, R.M., and Fierro, J.L.G. (2020). ZSM-5 zeolite based additive in FCC process: A review on modifications for improving propylene production. Catal. Surv. Asia *24*, 1–10. https://doi.org/10.1007/s10563-019-09285-1.

29. Mante, O.D., Agblevor, F.A., Oyama, S., and McClung, R. (2014). Catalytic pyrolysis with ZSM-5 based additive as co-catalyst to Y-zeolite in two reactor configurations. Fuel *117*, 649–659. https://doi.org/10.1016/j.fuel.2013.09.034.

30. Chen, H., Shen, B., and Pan, H. (2003). In situ formation of ZSM-5 in NaY gel and characterization of ZSM-5/Y composite zeolite. Chem. Lett. *32*, 726–727. https://doi.org/10.1246/cl.2003.726.

31. Wang, G., Liu, Y., Zheng, J., Pan, M., Zhang, H., Li, B., Yuan, S., Yi, Y., Tian, H., and Li, R. (2015). Zeolite–zeolite composite fabricated by polycrystalline Y zeolite crystals parasitizing ZSM-5 zeolite. J. Mater. Res. *30*, 2434–2446. https://doi.org/10.1557/jmr.2015.225.

32. Pan, M., Zheng, J., Liu, Y., Ning, W., Tian, H., and Li, R. (2019). Construction and practical application of a novel zeolite catalyst for hierarchically cracking of heavy oil. J. Catal. *369*, 72–85. https://doi.org/10.1016/j.jcat.2018.10.032.

33. Vermeiren, W., and Gilson, J.-P. (2009). Impact of zeolites on the petroleum and petrochemical industry. Top. Catal. *52*, 1131–1161. https://doi.org/10.1007/s11244-009-9271-8.

34. Mendoza-Castro, M.J., Qie, Z., Fan, X., Linares, N., and García-Martínez, J. (2023). Tunable hybrid zeolites prepared by partial interconversion. Nat. Commun. *14*, 1256. https://doi.org/10.1038/s41467-023-36502-3.

35. Mendoza-Castro, M.J., De Oliveira-Jardim, E., Ramírez-Marquez, N.T., Trujillo, C.A., Linares, N., and García-Martínez, J. (2022). Hierarchical Catalysts Prepared by Interzeolite Transformation. J. Am. Chem. Soc. *144*, 5163–5171. https://doi.org/10.1021/jacs.2c00665.

36. Qin, Z., Shen, B., Yu, Z., Deng, F., Zhao, L., Zhou, S., Yuan, D., Gao, X., Wang, B., Zhao, H., and Liu, H. (2013). A defect-based strategy for the preparation of mesoporous zeolite Y for high-performance catalytic cracking. J. Catal. *298*, 102–111. https://doi.org/10.1016/j.jcat.2012.11.023.

37. Verboekend, D., Vilé, G., and Pérez-Ramírez, J. (2012). Hierarchical Y and USY zeolites designed by post-synthetic strategies. Adv. Funct. Mater. *22*, 916–928. https://doi.org/10.1002/adfm.201102411.

38. Yan, Z., Ma, D., Zhuang, J., Liu, X., Liu, X., Han, X., Bao, X., Chang, F., Xu, L., and Liu, Z. (2003). On the acid-dealumination of USY zeolite: a solid state NMR investigation. J. Mol. Catal. Chem. *194*, 153–167. https://doi.org/10.1016/S1381-1169(02)00531-9.

39. Chen, K., Horstmeier, S., Nguyen, V.T., Wang, B., Crossley, S.P., Pham, T., Gan, Z., Hung, I., and White, J.L. (2020). Structure and Catalytic Characterization of a Second Framework Al(IV) Site in Zeolite Catalysts Revealed by NMR at 35.2 T. J. Am. Chem. Soc. *142*, 7514–7523. https://doi.org/10.1021/jacs.0c00590.

40. Auerbach, S.M., Carrado, K.A., and Dutta, P.K. (2003). Handbook of Zeolite Science and Technology, 1st ed. (CRC Press).

41. Groen, J.C., Peffer, L.A., and Pérez-Ramírez, J. (2003). Pore size determination in modified micro-and mesoporous materials. Pitfalls and limitations in gas adsorption data analysis. Microporous Mesoporous Mater. *60*, 1–17. https://doi.org/10.1016/S1387-1811(03)00339-1.

42. Qin, Z., Melinte, G., Gilson, J.P., Jaber, M., Bozhilov, K., Boullay, P., Mintova, S., Ersen, O., and Valtchev, V. (2016). The Mosaic Structure of Zeolite Crystals. Angew. Chem. *55*, 15049–15052. https://doi.org/10.1002/anie.201608417.

43. Šolcová, O., Matějová, L., Topka, P., Musilová, Z., and Schneider, P. (2011). Comparison of textural information from argon (87 K) and nitrogen (77 K) physisorption. J. Porous Mater. *18*, 557–565. https://doi.org/10.1007/s10934-010-9409-x.

44. Lupulescu, A.I., and Rimer, J.D. (2014). In situ imaging of silicalite-1 surface growth reveals the mechanism of crystallization. Science *344*, 729–732. https://doi.org/10.1126/science.1250984.

45. Daniell, W., Topsøe, N.-Y., and Knözinger, H. (2001). An FTIR study of the surface acidity of USY zeolites: Comparison of CO, CD3CN, and C5H5N probe molecules. Langmuir *17*, 6233–6239. https://doi.org/10.1021/la010345a.

46. Jin, F., and Li, Y. (2009). A FTIR and TPD examination of the distributive properties of acid sites on ZSM-5 zeolite with pyridine as a probe molecule. Catal. Today *145*, 101–107. https://doi.org/10.1016/j.cattod.2008.06.007.

47. Mlekodaj, K., Tarach, K., Datka, J., Góra-Marek, K., and Makowski, W. (2014). Porosity and accessibility of acid sites in desilicated ZSM-5 zeolites studied using adsorption of probe molecules. Microporous Mesoporous Mater. *183*, 54–61. https://doi.org/10.1016/j.micromeso.2013.08.051.

48. Lakiss, L., Vicente, A., Gilson, J.P., Valtchev, V., Mintova, S., Vimont, A., Bedard, R., Abdo, S., and Bricker, J. (2020). Probing the Brønsted Acidity of the External Surface of Faujasite-Type Zeolites. ChemPhysChem *21*, 1873–1881. https://doi.org/10.1002/cphc.202000062.

49. Liu, Y., Zhang, W., Liu, Z., Xu, S., Wang, Y., Xie, Z., Han, X., and Bao, X. (2008). Direct observation of the mesopores in ZSM-5 zeolites with hierarchical porous structures by laser-hyperpolarized 129Xe NMR. J. Phys. Chem. C *112*, 15375–15381. https://doi.org/10.1021/jp802813x.

50. Sharbini Kamaluddin, H., Gong, X., Ma, P., Narasimharao, K., Dutta Chowdhury, A., and Mokhtar, M. (2022). Influence of zeolite ZSM-5 synthesis protocols and physicochemical properties in the methanol-to-olefin process. Mater. Today Chem. *26*, 101061. https://doi.org/10.1016/j.mtchem.2022.101061.

51. Schulz, H., and Wei, M. (2014). Pools and constraints in methanol conversion to olefins and fuels on zeolite HZSM5. Top. Catal. *57*, 683–692. https://doi.org/10.1007/s11244-013-0225-9.

52. Wang, S., Qin, Z., Dong, M., Wang, J., and Fan, W. (2022). Recent progress on MTO reaction mechanisms and regulation of acid site distribution in the zeolite framework. Chem Catal. *2*, 1657–1685. https://doi.org/10.1016/j.checat.2022.05.012.

53. Khare, R., Liu, Z., Han, Y., and Bhan, A. (2017). A mechanistic basis for the effect of aluminum content on ethene selectivity in methanol-to-hydrocarbons conversion on HZSM-5. J. Catal. *348*, 300–305. https://doi.org/10.1016/j.jcat.2017.02.022.

54. Weissenberger, T., Machoke, A.G.F., Bauer, J., Dotzel, R., Casci, J.L., Hartmann, M., and Schwieger, W. (2020). Hierarchical ZSM-5 catalysts: The effect of different intracrystalline pore dimensions on catalyst deactivation behaviour in the MTO reaction. ChemCatChem *12*, 2461–2468. https://doi.org/10.1002/cctc.201902362.

55. Shi, Z., and Bhan, A. (2021). Tuning the ethylene-to-propylene ratio in methanol-to-olefins catalysis on window-cage type zeolites. J. Catal. *395*, 266–272. https://doi.org/10.1016/j.jcat.2022.07.035.

56. Schulz, H. (2018). About the mechanism of methanol conversion on zeolites. Catal. Lett. *148*, 1263–1280. https://doi.org/10.1007/s10562-018-2342-3.

57. Smirniotis, P.G., and Ruckenstein, E. (1994). Comparison of the Performance of ZSM-5, beta. Zeolite, Y, USY, and Their Composites in the Catalytic Cracking of n-Octane, 2, 2, 4-Trimethylpentane, and 1-Octene. Ind. Eng. Chem. Res. *33*, 800–813. https://doi.org/10.1021/ie00028a004.

58. Adewuyi, Y.G., Klocke, D., and Buchanan, J. (1995). Effects of high-level additions of ZSM-5 to a fluid catalytic cracking (FCC) RE-USY catalyst. Appl. Catal. Gen. *131*, 121–133. https://doi.org/10.1016/0926-860X(95)00124-7.

59. Yang, M., Fan, D., Wei, Y., Tian, P., and Liu, Z. (2019). Recent Progress in Methanol-to-Olefins (MTO) Catalysts. Adv. Mater. *31*, e1902181. https://doi.org/10.1002/adma.201902181.

60. Liang, T., Chen, J., Qin, Z., Li, J., Wang, P., Wang, S., Wang, G., Dong, M., Fan, W., and Wang, J. (2016). Conversion of methanol to olefins over H-ZSM-5 zeolite: reaction pathway is related to the framework aluminum siting. ACS Catal. *6*, 7311–7325. https://doi.org/10.1021/acscatal.6b01771.

61. Sousa, Z.S.B., Luna, A.S., Zotin, F.M.Z., and Henriques, C.A. (2022). Methanol-to-olefin conversion over ZSM-5: influence of zeolite chemical composition and experimental conditions on propylene formation. Chem. Eng. Commun. *209*, 623–635. https://doi.org/10.1080/00986445.2021.1884552.

62. Chen, J.Q., Bozzano, A., Glover, B., Fuglerud, T., and Kvisle, S. (2005). Recent advancements in ethylene and propylene production using the UOP/Hydro MTO process. Catal. Today *106*, 103–107. https://doi.org/10.1016/j.cattod.2005.07.178.

63. Gounder, R., Jones, A.J., Carr, R.T., and Iglesia, E. (2012). Solvation and acid strength effects on catalysis by faujasite zeolites. J. Catal. *286*, 214–223. https://doi.org/10.1016/j.jcat.2011.11.002.

64. Losch, P., Pinar, A.B., Willinger, M.G., Soukup, K., Chavan, S., Vincent, B., Pale, P., and Louis, B. (2017). H-ZSM-5 zeolite model crystals: Structure-diffusion-activity relationship in methanol-to-olefins catalysis. J. Catal. *345*, 11–23. https://doi.org/10.1016/j.jcat.2016.11.005.

65. Guisnet, M., and Magnoux, P. (2001). Organic chemistry of coke formation. Appl. Catal. Gen. *212*, 83–96. https://doi.org/10.1016/S0926-860X(00)00845-0.

66. Beyerlein, R., Choi-Feng, C., Hall, J., Huggins, B., and Ray, G. (1997). Effect of steaming on the defect structure and acid catalysis of protonated zeolites. Top. Catal. *4*, 27–42.

67. Occelli, M.L. (1991). Fluid Catalytic Cracking II: Concepts in Catalyst Design (American Chemical Society).

68. Narbeshuber, T.F., Vinek, H., and Lercher, J.A. (1995). Monomolecular conversion of light alkanes over H-ZSM-5. J. Catal. *157*, 388–395. https://doi.org/10.1006/jcat.1995.1304.

69. Beuque, A., Barreau, M., Berrier, E., Paul, J.-F., Batalha, N., Sachse, A., and Pinard, L. (2021). Transformation of dilute ethylene at high temperature on micro-and nano-sized H-ZSM-5 zeolites. Catalysts *11*, 282. https://doi.org/10.3390/catal11020282.